

Not All Attention Heads Are What You Need: Refining CLIP’s Image Representation with Attention Ablation

Feng Lin
Intellifusion Inc.

Marco Chen
Intellifusion Inc.

Haokui Zhang
Northwest Polytechnical University

Xiaotian Yu
Intellifusion Inc.

Guangming Lu
Harbin Institute of Technology

Rong Xiao
Intellifusion Inc.

Abstract

This paper investigates the role of attention heads in CLIP’s image encoder. Building on interpretability studies, we conduct an exhaustive analysis and find that certain heads, distributed across layers, are detrimental to the resulting representations. To mitigate their impact, we propose a simple yet effective Attention Ablation Technique (AAT) that suppresses selected heads by directly manipulating their attention weights. By incorporating two complementary strategies tailored to different application scenarios, AAT enables the systematic identification and ablation of harmful heads with minimal overhead. Experiments show that AAT consistently improves downstream performance across diverse domains, boosting recall by up to 11.1% on cross-modal retrieval benchmarks. These results highlight that AAT can effectively refine large-scale VLMs with virtually no extra inference cost, while yielding semantically meaningful patterns that align with existing interpretability findings.

1. Introduction

As a pioneering large-scale vision-language model (VLM), CLIP [28] has garnered widespread attention for its simple yet effective design and impressive capability across a wide range of downstream tasks [6, 16, 25, 42]. Early CLIP research focuses on advances in data [20], supervision [40], and architecture [16], recent studies have shifted toward analyzing its learned representations [1, 11, 18]. These efforts aim to uncover the intrinsic characteristics of CLIP’s representations, providing insights for further enhancement.

A recent interpretability study [11] investigates CLIP’s image representations by decomposing them across attention heads, revealing strong correlations between specific heads and particular linguistic concepts. Through manually

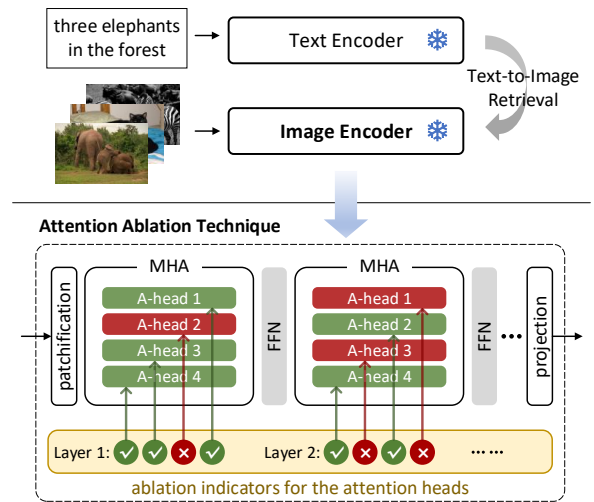


Figure 1. An illustration of AAT-improved CLIP for text-to-image retrieval. “A-head i ” denotes the i -th head in MHA. With model weights frozen, AAT ablates the selected image encoder’s heads. Cross marks denote head ablation while check marks for retention.

removing those heads associated with spurious cues in the last four transformer layers, it improves CLIP’s image representations for a targeted zero-shot classification task. This finding suggests that individual head makes distinct contribution to output representations, acting as property-specific “filters” over visual concepts. Building on this insight, we systematically extend the analysis to all attention heads in CLIP’s image encoder across diverse downstream tasks.

Trained on vast amounts of internet-sourced image–text pairs, CLIP models probably develop attention heads that encode task-irrelevant signals—such as domain biases or spurious cues—that may hinder downstream performance. Some heads may also overfit to noise inherent in uncurated training data. Such detrimental heads can appear through-

out the transformer layers of the image encoder. We hypothesize that ablating them can refine the output and thereby yield consistent gains across diverse downstream tasks.

To verify our hypothesis, we conduct a preliminary experiment to assess the impact of individual attention heads. We find that ablating even a single detrimental head can enhance CLIP’s downstream performance, with further gains from ablating simple combinations of negatively impactful heads. Inspired by this, we develop an efficient Attention Ablation Technique (AAT) that refines the representations by evicting groups of detrimental heads. It formulates the problem as a combinatorial optimization task, solved using either Genetic Algorithm (GA) or Back-Propagation (BP).

The key difference between GA-based AAT (AAT-GA) and BP-based AAT (AAT-BP) lies in how they identify detrimental attention heads. AAT-GA uses a fitness function that measures the distance between positive image–text pairs and hard negative pairs, whereas AAT-BP introduces a lightweight training scheme with a learnable gating parameter for each head to assess its relevance. Both strategies yield substantial gains on multi-domain retrieval and classification tasks, with their respective strengths making them suitable for different deployment scenarios.

AAT leaves CLIP’s parameters unchanged and instead operates by manipulating the attention weights of selected heads, as illustrated in Figure 1. It suppresses the weights on image tokens while correspondingly amplifying the class token weight, ensuring that ablated heads contribute minimally to the output representation. As an agile and versatile technique, AAT is particularly well suited to resource-constrained scenarios, like limited compute or scarce high-quality data, while preserving strong generalization across diverse domains. The main contributions as follows:

- We extensively explore the impacts of attention heads in CLIP’s image encoder and show that ablating detrimental heads improves representation quality. To our knowledge, this is the first systematic study of refining CLIP’s outputs by probing the impact of individual attention heads.
- We introduce AAT, a simple yet effective method for automatically identifying and ablating detrimental attention heads without altering original model weights, offering two variants tailored to different application scenarios.
- AAT delivers consistent and substantial gains across diverse downstream tasks, improving recall by up to 11.1% on retrieval benchmarks with negligible extra overhead.
- Our result analysis provides concrete evidence that attention heads are semantically meaningful, reinforcing and extending existing interpretability findings of VLMs.

2. Related Work

The Interpretability of CLIP’s Representation Recent studies investigate CLIP’s representations from various perspectives. [26] analyzes entanglement between words and

indices	11-6	10-7	10-9	9-9	11-0	vanilla
mean-R	81.1	80.8	80.8	80.7	80.7	79.9

Table 1. Top five single-head ablation configurations for text-to-image retrieval on COCO-CN *val* set [21]. “*m-n*” demotes the *n*-th head in the *m*-th layer. Evaluations are based on CLIP-ViT-B [36], mean-R (the mean of R@1, R@5, and R@10) as metric.

Models	<i>val</i>	<i>test</i>	<i>all</i>
vanilla CLIP [36]	79.9	81.1	41.7
naive joint head ablation	82.5	82.6	43.2

Table 2. Comparison of mean-R for text-to-image retrieval on the COCO-CN *val*, *test* and *all* set.

images. [22] presents a semantic shift toward background regions. [31] finds a strong connection between the modality gap and the loss local minima. [41] improves image-text matching explainability via gradients and heatmaps. [7] finds that CLIP exhibits distinctive outlier features tied to ImageNet shift robustness. Most closely related to AAT, [3] boosts interpretability by converting dense embeddings into sparse, concept-based ones, and [11] reveals spatial localization and property-specific roles of attention heads.

Attention Weight Manipulation Attention mechanism is central to Transformers [4], and manipulating attention weights in trained models has shown notable benefits. Prior heuristic method calibrates its weights toward hidden attention sinks in LLMs [38]; reformulates attention for segmentation [18]; reweights semantic tokens to refine text embeddings [17]; and amplifies image-token weights to mitigate hallucinations in VLMs [24]. AAT is conceptually related to them but introduces a novel, empirically grounded manipulation strategy based on attention-head behaviors.

Attention Head Pruning in LMs The idea behind AAT parallels early works on language models [2, 27, 33], which reveal redundancy among attention heads. Those methods typically prune heads to slim models with modest accuracy loss. Though head pruning is well established for LMs, its study to much compact VLMs remains underexplored.

Parameter-Efficient Finetuning AAT-BP is superficially similar with PEFT [13, 14, 19, 32, 34]—requiring only hundreds of learnable gates—but, unlike PEFT’s largely black-box updates, each parameter in AAT-BP is explicitly interpretable. It is also far more parameter-efficient, requiring orders of magnitude fewer parameters than PEFT [9].

3. The Impact of Individual Attention Heads

As a preliminary step, we conduct a simple head-wise ablation sweep of CLIP’s image encoder. Using AAT (described in Section 4.1), we ablate one attention head at a time and

evaluate cross-modal retrieval performance. For ViT-B with 144 heads across 12 layers, this yields 144 results, several of which outperform the original baseline. The top 5 highest-performing configurations are ranked in Table 1, with full results in Appendix 8. Remarkably, ablating even a single detrimental head can raise mean recall by up to 1.2%.

Building on this observation, we ablate the direct union of all the individually identified detrimental heads—those whose single-head ablation improves recall. As shown in Table 2, this naive combination consistently boosts retrieval performance across multiple test subsets. Notably, although these heads are selected independently, their joint ablation yields further gains. This motivates us to develop more principled strategies for optimal head selection.

4. Attention Ablation Technique

We introduce AAT in this section. Section 4.1 explains the method for ablating individual attention heads. Sections 4.2 and 4.3 present two alternative strategies—GA and BP—for identifying a globally optimal set of detrimental heads, with each strategy tailored to different application scenarios.

4.1. Ablating a Single Attention Head

A transformer layer consists of a multi-head attention module (MHA) and a feed-forward network (FFN) [10]. For the CLIP’s image encoder, the input token sequence of length N is composed of a leading class token followed by $N - 1$ image tokens. Let x_h^l represent the input to the h -th attention head of MHA in the l -th transformer layer. The output of each head, y_h^l , can be formulated as follows:

$$\mathcal{A}_h^l = \text{Softmax}\left(\frac{f_q(LN(x_h^l)) \cdot f_k(LN(x_h^l)^T)}{\sqrt{d_k}}\right), \quad (1)$$

$$y_h^l = \mathcal{A}_h^l \cdot f_v(LN(x_h^l)) \quad (2)$$

where f_q , f_k , and f_v denote projection layers for queries, keys, and values, respectively. LN refers to LayerNorm, d_k is the embedding dimension of each head, and \mathcal{A}_h^l denotes the attention weight matrix with dimensions $N \times N$.

As shown in the formulations above, the attention weight matrix \mathcal{A} is produced by a softmax function, ensuring that each row sums to 1. The output of each attention head, y , is then obtained by multiplying \mathcal{A} with the projected values. To ablate a specific head, we manipulate \mathcal{A} to suppress the contribution of image tokens to the output representation, as illustrated in Figure 2. Specifically, this involves two steps:

1. Reducing the importance of image tokens: Modify \mathcal{A} as $\mathcal{A}[:, j] \leftarrow \mathcal{A}[:, j] \times \beta$, where $j \in \{1, 2, \dots, N - 1\}$.
2. Renormalizing each row of \mathcal{A} : Scale \mathcal{A} as $\mathcal{A}[i, j] \leftarrow \mathcal{A}[i, j] / \mathcal{A}_i$, where $i, j \in \{0, 1, \dots, N - 1\}$ and $\mathcal{A}_i = \sum_j \mathcal{A}[i, j]$, to preserve the row-wise normalization.

A hyper-parameter β controls the degree of suppression applied to image-token weights; unless otherwise stated, we

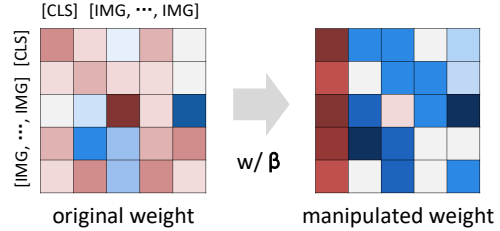


Figure 2. The left 5×5 matrix shows the original attention weight, while the right depicts it after manipulation. CLS and IMG denote the class token and an image token, respectively, with a total length of 5. Darker blue indicates lower attention scores (approaching zero), while darker red indicates higher scores (approaching one).

set $\beta = 0.1$. After these two steps, the modified attention weight replaces the original, while all other MHA operations remain unchanged. This allows refinement of the output representation without altering the model parameters.

4.2. AAT with Genetic Algorithm

As discussed in Section 3, ablating detrimental heads in CLIP’s image encoder can refine its output representations. Our goal is to identify the optimal subset of such heads. We formulate this as a combinatorial optimization problem and solve it using a small validation set \mathcal{D} containing a limited number of image–text pairs. To efficiently explore the large search space, we employ a Genetic Algorithm (GA) [12], which evolves candidate solutions over generations to discover high-quality configurations.

Specifically, we represent all attention heads in the image encoder as a binary vector, where each element corresponds to a head (1 for ablated, 0 for retained). Using the validation set \mathcal{D} , the GA optimizes this vector configuration. To align with CLIP’s training objective which brings matching image–text pairs closer while pushing mismatched pairs apart, we design a fitness function \mathcal{F} that reflects this property. \mathcal{F} serves as the optimization target and is defined as follows:

$$\mathcal{F} = \frac{1}{N} \sum_{i=1}^N (S_{pos}^i - \max_{j \in \mathcal{H}^i} (S_{neg}^{i,j})) \quad (3)$$

where N is the number of sample pairs in \mathcal{D} . S_{pos}^i denotes the cosine similarity between the i -th text and its ground-truth image. $S_{neg}^{i,j}$ denotes the cosine similarity between the i -th text and the j -th image in \mathcal{H}^i (an updatable set of hard negatives for the i -th text), which is detailed below.

We first evaluate vanilla CLIP on \mathcal{D} for text-to-image retrieval. For each text query i , we collect the top k_1 non-matching images (false positives) as hard negatives to initialize \mathcal{H}^i . To avoid overfitting, we augment \mathcal{H}^i with k_2 randomly sampled non-matching images from \mathcal{D} and refresh these k_2 samples at the end of each GA generation. This dynamic \mathcal{H} is crucial to AAT-GA: it encourages larger

tasks		text-to-image retrieval								image-to-text retrieval							
splits		the <i>test</i> set				the <i>all</i> set				the <i>test</i> set				the <i>all</i> set			
size	method	R@1	R@5	R@10	mR	R@1	R@5	R@10	mR	R@1	R@5	R@10	mR	R@1	R@5	R@10	mR
B	vanilla	38.8	64.2	73.8	58.9	13.0	26.5	33.8	24.4	57.8	81.7	88.6	76.0	24.2	43.1	52.1	39.8
	AAT-GA	41.3	66.7	76.6	61.5	14.0	28.3	35.9	26.1	60.3	82.7	89.3	77.4	26.0	45.4	54.4	41.9
	AAT-BP	40.5	66.2	75.9	60.9	13.9	28.1	35.6	25.9	58.9	82.5	89.5	77.0	24.8	44.2	53.1	40.7
L	vanilla	43.9	68.8	78.3	63.7	16.1	31.3	39.1	28.8	59.5	82.3	89.2	77.0	25.5	44.9	53.9	41.4
	AAT-GA	46.3	71.3	80.8	66.1	17.4	33.3	41.4	30.7	62.8	84.2	90.2	79.1	27.6	47.9	56.8	44.1
	AAT-BP	46.0	71.8	80.9	66.2	17.2	33.2	41.3	30.6	60.6	83.3	89.7	77.8	25.6	45.6	54.7	42.0
H	vanilla	47.4	72.1	80.9	66.8	18.5	34.8	42.9	32.1	60.6	84.6	90.9	78.7	26.0	46.1	55.4	42.5
	AAT-GA	49.3	74.1	82.7	68.7	19.5	36.5	44.7	33.6	63.8	85.8	91.5	80.4	28.2	48.7	58.1	45.0
	AAT-BP	48.6	73.5	82.2	68.1	19.1	35.9	44.1	33.0	63.7	85.9	91.5	80.4	28.1	48.8	58.0	45.0

Table 3. Comparison on MS COCO for cross-modal retrieval. R@k denotes recall rate at rank k, and mR (mean-R) denotes the average of R@1, R@5, and R@10. Model sizes are denoted as B (ViT-B), L (ViT-L), and H (ViT-H). Best results are highlighted in bold.

margins between true matches and evolving hard negatives while continuously incorporating newly challenging cases.

In Eq. 3, the first term of \mathcal{F} rewards similarity between true image-text pairs, while the second penalizes similarity to the hardest negatives in \mathcal{H} . Combined with standard crossover and mutation, this objective steers the GA toward an optimal (or near-optimal) head selection for ablation.

Application Scenarios AAT-GA operates entirely at inference, making it well suited to resource-constrained deployments. It can run on the low-power, inference-oriented edge devices with limited-precision compute capabilities, such as INT8/INT16 chips (e.g., Google Coral Edge TPU, Ethos-N78, Mythic M1108 AMP). It is also data-efficient, requiring only a small validation set for optimization (Section 5.4.2), whereas supervised finetuning (SFT) tends to overfit in such settings (Appendix 12).

4.3. AAT with Back-Propagation

Since GA may require more inference trials when poorly initialized, in addition, not all resource-constrained settings lack floating-point compute, thus we introduce a gradient-based alternative: Back-Propagation (AAT-BP). Rather than using the uniform suppression factor β in AAT-GA, AAT-BP assigns each probed head a learnable parameter α_i . We map α_i to a head-specific suppression factor $\beta_i \in [0, 1]$ that controls the ablation strength of head i , replacing β with β_i . Formally, β_i is defined as:

$$\beta_i = \text{Sigmoid}(\tau \cdot \alpha_i) \quad (4)$$

where the temperature $\tau > 1$ sharpens the sigmoid, encouraging β_i to approach extreme values (0 or 1) during optimization. Empirically, we set $\tau = 5.0$ and initialize each α_i to 1.0, yielding β_i near 1 at the start. As in AAT-GA, we optimize α_i on the same validation set \mathcal{D} using CLIP’s contrastive supervision objective.

Application Scenarios While BP might get stuck to local optima, its rapid convergence makes it practical and efficient in real-world use. Its low compute and data demands

further suit resource-limited settings. In spirit, AAT-BP resembles PEFT, yet it uses orders of magnitude fewer learnable parameters than typical PEFT [13, 14], a level of efficiency enabled by targeted manipulation of attention heads.

5. Experiments

5.1. Experimental Settings

5.1.1. Models

We evaluate AAT using CLIP [28] and Chinese-CLIP [36], across ViT-B, ViT-L, and ViT-H. Specifically, we use OpenCLIP released models [15] trained on LAION-2B (a subset of LAION-5B [30]) and Chinese-CLIP released models trained on 200M Chinese image-text pairs.

5.1.2. AAT Optimization Data

As introduced in Sections 4.2 and 4.3, we use a small validation set \mathcal{D} to optimize AAT. For CLIP, we randomly sample 1k image-text pairs from the MS COCO *train* set as \mathcal{D} . For Chinese-CLIP, we directly use the COCO-CN *val* set that contains 1k image-text pairs.

5.1.3. AAT-GA Implementation

The key hyper-parameters for GA are configured as follows: the population size is determined by the number of heads—48 for ViT-B, 96 for ViT-L, and 128 for ViT-H. A two-point crossover is applied with a probability of 0.9, while mutation occurs with a probability of 0.5 using the flip-bit strategy. The tournament selection with a size of 3 is employed. The evolution proceeds for up to 100 generations, with early stopping triggered when fitness gains plateau or population diversity becomes low.

5.1.4. AAT-BP Implementation

The BP optimization settings are as follows: learning rate of $2e-2$ for CLIP and $5e-2$ for Chinese-CLIP, with a batch size of 256. ViT-B models are trained for 32 epochs, and larger models for 64. All other hyper-parameters follow the OpenCLIP codebase [15].

tasks		text-to-image retrieval								image-to-text retrieval							
splits		the <i>test</i> set				the <i>all</i> set				the <i>test</i> set				the <i>all</i> set			
size	method	R@1	R@5	R@10	mR	R@1	R@5	R@10	mR	R@1	R@5	R@10	mR	R@1	R@5	R@10	mR
B	vanilla	67.20	88.68	93.06	82.98	30.54	52.17	61.27	47.99	85.90	97.90	99.10	94.30	48.16	72.76	81.18	67.36
	AAT-GA	70.26	90.06	94.42	84.91	32.64	54.90	64.04	50.53	87.20	97.10	98.90	94.40	50.47	74.09	81.89	68.82
	AAT-BP	69.76	90.08	93.96	84.60	32.69	54.79	63.98	50.49	86.30	97.70	99.00	94.33	49.58	73.77	81.97	68.44
L	vanilla	73.52	91.84	95.36	86.91	36.26	58.98	67.91	54.39	87.00	98.20	99.50	94.90	48.90	74.39	83.09	68.79
	AAT-GA	75.74	92.72	95.92	88.13	38.28	61.16	69.93	56.46	88.10	98.50	99.40	95.33	52.68	76.96	84.90	71.51
	AAT-BP	76.20	93.12	95.96	88.43	38.47	61.75	70.62	56.95	87.50	98.10	99.40	95.00	50.89	75.71	83.70	70.10
H	vanilla	76.10	93.44	96.42	88.65	41.18	64.03	72.61	59.27	88.60	98.70	99.60	95.63	51.10	77.44	85.64	71.39
	AAT-GA	77.84	94.50	96.94	89.76	43.10	66.20	74.51	61.27	90.40	98.90	99.60	96.30	54.98	80.06	87.51	74.18
	AAT-BP	77.78	94.48	96.92	89.73	42.62	65.78	74.32	60.91	90.70	98.90	99.60	96.40	56.16	80.79	88.05	75.00

Table 4. Comparison on Flickr30k for cross-modal retrieval. The symbols in the table have the same meaning as those in Table 3.

types	natural images											non-natural images			
tasks	ACT	CEL	COL	CNT	FIG	OBJ	OCR	POS	SCE	mean	CR	NC	TT	mean	
vanilla	73.6	74.0	73.4	59.8	82.8	79.6	77.0	65.8	87.0	74.8	27.7	21.0	2.7	17.1	
AAT-GA	75.8	77.7	76.8	60.4	86.4	81.4	81.3	67.4	89.0	77.4	20.3	21.3	2.3	14.6	
AAT-BP	74.8	77.0	76.2	60.6	86.6	83.0	79.7	71.6	88.0	77.5	22.3	18.3	2.3	14.3	

Table 5. Text-to-image retrieval results on ReCoS using ViT-B, evaluated with R@1 as the metric.

5.1.5. Benchmarks

We evaluate AAT-improved CLIP upon MS COCO [23], Flickr30k [37], and ReCoS [5], and assess AAT-improved Chinese-CLIP on two widely-used Chinese retrieval benchmarks: COCO-CN [21] and Flickr30k-CNA [35]. For MS COCO, Flickr30k, COCO-CN, Flickr30k-CNA, we report results on two splits: the *test* split (the original test set) and the *all* split (all samples in the dataset), enabling a comprehensive large-scale retrieval analysis. We further evaluate zero-shot classification on the ImageNet-1k *val* set [8]. Dataset and metric details are provided in Appendix 7.

5.1.6. Baseline

Aside from vanilla CLIP, we also compare AAT to two recent strong PEFT baselines, namely CLIP-LoRA [39] and ReFT [34]. Detailed settings for both are as follows.

Vanilla CLIP The vanilla CLIP and Chinese-CLIP models with their original, unmodified weights (prior to any improvement via AAT) serve as our primary baselines.

CLIP-LoRA For fairness, we apply LoRA (using rank 1 or 2) to the Q/K projections of each head from image encoder, mirroring AAT’s intervention points. To better match AAT-BP’s parameter count, we also include a light-weight variant (LoRA-lite) that targets only the final image encoder layer. We adopt CLIP-LoRA’s training setup: learning rate $2e-4$, batch size 32, and 64 epochs (chosen via search).

ReFT Following the paper, we use rank 4 for the low-rank projection R . A preparatory search over intervention positions shows that applying ReFT to all tokens slightly outperforms restricting it to the class token or the top-5 tokens for

CLIP (contrary to some LLM findings). For completeness, we implement both DiReFT and LoReFT across all image-encoder layers, and parameter-reduced variants (DiReFT- / LoReFT-lite) applied only to the last layer. We train with learning rate $2e-5$ and batch size 32 (higher rates tend to collapse R), for 96 epochs until accuracy saturates.

5.2. Compared with Vanilla CLIP

5.2.1. Cross-modal Retrieval

MS COCO Table 3 reports MS COCO results for text-to-image and image-to-text retrieval with AAT-GA and AAT-BP. For text-to-image, GA and BP perform comparably, with mean-R differences under 1%. On the *test* set, AAT yields a 1.3%~2.6% gains in mean-R across model sizes, and over 1.5% on average for the *all* set. For image-to-text, AAT achieves a 0.8%~2.1% mean-R gain on the *test* set and 0.6%~2.7% on the *all* set.

Flickr30k Table 4 reports Flickr30k results. For text-to-image, AAT presents a 1.08%~1.93% mean-R improvement on the *test* set and 1.64%~2.56% on the *all* set. Notably, gains on the *test* set tend to diminish at higher recall levels, likely due to saturation. A similar trend can be observed for image-to-text retrieval as well, yet with consistent mean-R improvements of 0~0.8% on the *test* set and 1.08%~3.61% on the *all* set.

ReCoS To evaluate broader effectiveness, Table 5 reports text-to-image retrieval on the challenging ReCoS, spanning 12 subsets across diverse domains (subset abbreviations in Appendix 7). We group subsets by image domain: natural (*e.g.*, landscapes, animals, movie scenes, profile photos) and non-natural (*e.g.*, code snippets, characters, formulas)

tasks		text-to-image retrieval								image-to-text retrieval							
splits		the <i>test</i> set				the <i>all</i> set				the <i>test</i> set				the <i>all</i> set			
size	method	R@1	R@5	R@10	mR	R@1	R@5	R@10	mR	R@1	R@5	R@10	mR	R@1	R@5	R@10	mR
B	vanilla	62.2	86.9	94.3	81.1	24.0	45.4	55.8	41.7	56.2	83.8	93.4	77.8	22.6	43.0	52.7	39.4
	AAT-GA	64.9	89.9	96.5	83.8	27.6	50.0	60.4	46.0	62.6	89.0	95.3	82.3	25.5	47.1	57.2	43.3
	AAT-BP	66.0	90.7	96.3	84.3	27.4	50.4	60.6	46.1	63.1	90.4	95.6	83.0	26.2	48.3	58.1	44.2
L	vanilla	63.9	88.7	94.5	82.4	26.7	48.6	58.5	44.6	60.4	84.2	93.3	79.3	24.4	44.6	54.5	41.2
	AAT-GA	66.5	91.4	96.1	84.7	30.1	52.9	63.2	48.7	65.9	89.0	95.4	83.4	29.8	51.6	61.6	47.7
	AAT-BP	68.2	91.1	96.6	85.3	30.2	52.9	63.3	48.8	67.3	90.6	96.9	84.9	30.4	52.8	63.5	48.9
H	vanilla	69.6	89.9	95.8	85.1	30.4	52.4	62.2	48.3	63.1	86.7	93.0	80.9	26.3	46.5	56.0	42.9
	AAT-GA	72.3	92.3	96.5	87.0	33.8	56.8	66.6	52.4	66.6	89.0	94.5	83.4	30.0	51.1	60.4	47.1
	AAT-BP	73.7	92.7	97.6	88.0	35.5	59.4	69.1	54.7	72.4	93.1	97.3	87.6	35.4	58.4	68.3	54.0

Table 6. Comparison on COCO-CN for cross-modal retrieval. The symbols in the table have the same meaning as those in Table 3.

tasks		text-to-image retrieval								image-to-text retrieval							
splits		the <i>test</i> set				the <i>all</i> set				the <i>test</i> set				the <i>all</i> set			
size	method	R@1	R@5	R@10	mR	R@1	R@5	R@10	mR	R@1	R@5	R@10	mR	R@1	R@5	R@10	mR
B	vanilla	62.12	86.62	92.52	80.42	24.35	44.78	54.36	41.16	73.70	93.20	97.00	87.97	33.45	56.84	66.56	52.28
	AAT-GA	65.60	89.04	94.18	82.94	26.79	48.20	57.91	44.30	77.70	95.90	97.50	90.37	36.76	60.51	70.10	55.79
	AAT-BP	66.58	89.28	94.36	83.41	27.68	49.51	59.17	45.45	78.60	95.50	97.90	90.67	37.18	61.46	71.07	56.57
L	vanilla	67.58	89.52	94.28	83.79	28.79	50.39	59.80	46.33	80.00	96.50	98.20	91.57	37.15	61.59	71.05	56.59
	AAT-GA	71.48	91.60	95.52	86.20	32.45	55.02	64.51	50.66	87.00	97.60	98.90	94.50	45.17	69.78	78.53	64.50
	AAT-BP	70.90	91.34	95.70	86.00	31.69	54.46	64.10	50.08	87.50	97.40	99.10	94.67	44.25	69.05	77.82	63.71
H	vanilla	70.94	91.30	95.30	85.85	33.92	56.27	65.38	51.86	81.40	97.00	98.90	92.43	42.35	66.47	75.43	61.42
	AAT-GA	74.86	93.00	96.50	88.12	37.54	60.46	69.47	55.82	85.40	98.10	99.00	94.17	48.23	72.16	80.29	66.89
	AAT-BP	75.30	93.40	96.78	88.49	37.64	60.68	69.64	55.99	88.60	97.50	99.30	95.13	52.12	75.71	83.38	70.40

Table 7. Comparison on Flickr30k-CNA for cross-modal retrieval. The symbols in the table have the same meaning as those in Table 3.

that are typically synthetic with uniform backgrounds.

AAT consistently outperforms on natural subsets, with a mean R@1 gain of around 3%. However, its performance declines on non-natural images. We attribute this drop to two main factors: (1) significant domain shifts between the test images and those used to identify detrimental attention heads (see Appendix 13); and (2) the inherent limitations of CLIP models. Tasks such as CR (code reasoning), NC (numerical calculation), and TT (text translation) demand beyond visual perception, but understanding and reasoning capabilities that CLIP is not explicitly trained for.

COCO-CN Table 6 reports the COCO-CN results. For text-to-image retrieval, AAT achieves a 1.9%~3.2% higher mean-R across model sizes using both GA and BP on the *test* set, while the gain is even more pronounced, reaching up to 6.4%, on the *all* set. For image-to-text retrieval, AAT delivers a 2.5%~6.7% improvement on the *test* set and 3.9%~11.1% on the *all* set. These advances surpass those observed in CLIP, suggesting its effectiveness is correlated with the quality of the original representations.

Flickr30k-CNA Table 7 presents the Flickr30k-CNA results. AAT improves mean-R for text-to-image retrieval by 2.21%~3.2% on the *test* set and 3.14%~4.33% on the *all* set. For image-to-text, it outperforms the baseline by 3% on the *test* set and up to 8.98% on the *all* set. Consistent with COCO-CN, AAT delivers greater gains for Chinese-CLIP.

5.2.2. Zero-shot Classification

Since AAT is primarily designed for retrieval, we extend its application to zero-shot classification on ImageNet-1k, with minimal but essential adaptation. We identify a mismatch between the text templates used in ImageNet-1k classification (*e.g.*, “a photo of a CLASS_NAME”) and the natural language captions in the original optimization set \mathcal{D} (*e.g.*, “An old woman sits on a bench”). To resolve this, we construct a new \mathcal{D} by incorporating 500 image-text pairs from the ImageNet-1k training set that follow the zero-shot template style, and re-run AAT on CLIP using this adapted \mathcal{D} .

We test the resulting models on the ImageNet-1k *val* set and observe consistent top-1 accuracy gains of 1%~1.5% (Table 9). To further assess generalization, we test retrieval on MS COCO and Flickr30k. Performance remains strong, with no noticeable degradation relative to models optimized on the original \mathcal{D} (Tables 3 and 4); text-to-image differences are under 0.6% on MS COCO and 0.3% on Flickr30k.

5.3. Compared with PEFT

Table 8 reports recall for text-to-image and image-to-text retrieval on MS COCO and Flickr30k, along with the number of additional learnable parameters.

5.3.1. AAT vs. LoRA.

In general, AAT achieves comparable recall performance to LoRA: the average mean-R difference on both MS COCO and Flickr30k is less than 0.5%. In terms of parameter efficiency, AAT-GA adds no learnable parameters, and AAT-

	ViT-B						ViT-L						ViT-H					
	#param	MS COCO		Flickr30k		Avg	#param	MS COCO		Flickr30k		Avg	#param	MS COCO		Flickr30k		Avg
		T2I	I2T	T2I	I2T			T2I	I2T	T2I	I2T			T2I	I2T			
vanilla	n/a	58.9	76.0	82.98	94.30	78.05	n/a	63.7	77.0	86.91	94.90	80.63	n/a	66.8	78.7	88.65	95.63	82.45
AAT-GA	0	61.5	77.4	84.91	94.40	79.55	0	66.1	79.1	88.13	95.33	82.17	0	68.7	80.4	89.76	96.30	83.79
AAT-BP	144	60.9	77.0	84.60	94.33	79.21	384	66.2	77.8	88.43	95.00	81.86	512	68.1	80.4	89.73	96.40	83.66
LoRA-lite	3.1k	59.2	76.3	83.23	94.10	78.21	4.1k	64.2	77.4	87.28	94.60	80.87	5.1k	67.2	79.0	88.83	95.60	82.66
LoRA (r=1)	36.9k	62.2	77.2	85.39	93.63	79.61	98.3k	65.8	78.7	88.04	95.27	81.95	163.8k	68.7	79.9	89.93	96.10	83.66
LoRA (r=2)	73.8k	62.7	77.5	85.73	93.98	79.98	196.6k	66.4	78.6	88.29	95.22	82.13	327.5k	69.1	80.3	89.85	96.40	83.91
DiReFT-lite	6.1k	60.1	75.7	83.82	93.83	78.36	8.2k	64.3	76.9	87.32	94.43	80.74	10.2k	67.1	78.9	88.91	95.90	82.70
DiReFT	73.8k	62.0	76.3	85.18	93.50	79.25	196.6k	65.7	77.4	88.16	94.50	81.44	327.5k	68.9	78.6	89.95	95.50	83.24
LoReFT-lite	6.1k	59.9	75.2	83.49	93.73	78.08	8.2k	64.3	77.1	87.11	94.53	80.76	10.2k	67.0	78.4	88.67	94.27	82.09
LoReFT	73.8k	61.1	75.2	84.70	93.93	78.73	196.6k	65.4	76.7	87.76	94.10	80.99	327.5k	67.8	78.3	89.47	95.33	82.73

Table 8. Mean-R comparison for text-to-image (T2I) and image-to-text (I2T) retrieval across base, large, and huge model variants.

datasets	ImageNet-1k			MS COCO			Flickr30k		
	B	L	H	B	L	H	B	L	H
vanilla	68.12	72.62	76.17	58.9	63.7	66.8	82.98	86.91	88.65
AAT-GA	69.17	74.11	77.28	61.2	65.8	68.6	84.67	88.02	89.67
AAT-BP	69.01	73.76	77.25	61.0	65.6	68.2	84.42	88.34	89.61

Table 9. Top-1 accuracy on ImageNet-1k *val* set for zero-shot classification, and mean-R on MS COCO and Flickr30k *test* sets.

BP uses only hundreds, whereas LoRA requires two orders of magnitude more (roughly $250 \times \sim 600 \times$) than AAT-BP. When constrained to a closely comparable parameter budget (LoRA-lite, $10 \times$ AAT-BP), LoRA’s performance degrades substantially. These results underscore AAT’s strong parameter efficiency, making it well-suited for the resource-constrained platforms.

5.3.2. AAT vs. ReFT.

Overall, AAT surpasses DiReFT and LoReFT across different model sizes. In detail, AAT outperforms the DiReFT-lite and LoReFT-lite, even though these two variants require $20 \times \sim 40 \times$ more parameters, by 1.1~1.4 mean-R on average across base, large, and huge models. It still slightly exceeds the full ReFT variants that use about $500 \times$ more parameters. Although ReFT is often more parameter-efficient than LoRA in LLMs, these CLIP results invert this trend. Given that our LoRA setup targets Q/K projections (implicitly modifying the attention weights), we conjecture that, for compact VLMs, attention manipulation is a more effective lever than downstream representation intervention.

5.4. Ablation Study

5.4.1. The Value of β

We empirically set $\beta = 0.1$ in AAT-GA and examine its effect on performance. Figure 3 plots mean-R on the COCO-CN *all* set as β decreases from 1 to 0.02: performance rises, peaks at $\beta = 0.1$, then declines. For AAT-BP, we analyze the head-specific β values obtained by applying a sigmoid (with temperature τ) to the learnable α parameters. Deeper layers exhibit more polarized β (near 0 or 1), whereas shallower layers remain closer to the initial value of 1. This

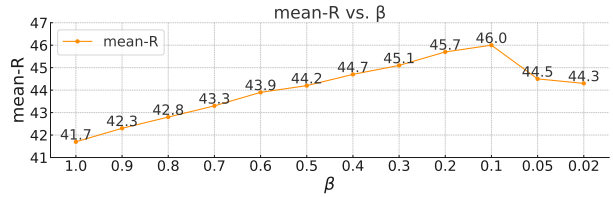


Figure 3. Mean-R for text-to-image retrieval on the COCO-CN *all* set vs. β values in AAT-GA, using the ViT-B-based model.

suggests depth-dependent gradient propagation during BP, which may account for the result differences between AAT-GA and AAT-BP in certain cases.

5.4.2. The Size of D

We study the effect of the validation set size for AAT optimization. Starting from \mathcal{D} with 1k image-text pairs, we randomly sample subsets of 500, 200, and 100 pairs and report mean-R for both CLIP and Chinese-CLIP in Table 10. Even with only 100 pairs, AAT surpasses the baseline (size = 0) by 1% on CLIP and 3% on Chinese-CLIP. As increasing the size to 500, it yields only marginal additional gains.

5.4.3. Selection of AAT Optimization Data

As described in Section 5.1.2, we optimize AAT on a 1k subset from MS COCO or COCO-CN. To examine the effect of used data and potential domain bias, we construct an in-domain \mathcal{D} using 1k Flickr30k-CNA *val* image-text pairs. We then re-run AAT with this in-domain set and compare Flickr30k-CNA performance to AAT optimized on COCO-CN. As shown in Table 11, using in-domain data yields only marginal gains (typically $< 0.5\%$), indicating strong cross-domain generalization of AAT-refined representations.

5.5. AAT Optimization Runtime

We optimize AAT on $8 \times$ NVIDIA RTX 4090 GPUs with an Intel(R) Xeon(R) Platinum 8358P @ 2.60GHz platform. To demonstrate real-world feasibility, we list wall-clock runtime and GPU-hours under the standard setup in Section 5.1 (see the 4th–5th columns of Table 13). While GA is attractive for low-precision (INT8/INT16) inference hardware, as

the size of \mathcal{D}		0	100	200	500	1000
CLIP	AAT-GA	24.4	25.4	25.7	26.0	26.1
	AAT-BP	24.4	25.2	25.4	25.7	25.9
Chinese-CLIP	AAT-GA	41.7	45.1	45.3	45.9	46.0
	AAT-BP	41.7	44.7	45.2	45.7	46.1

Table 10. Mean-R vs. the size of \mathcal{D} : CLIP is evaluated on the MS COCO *all* set, and Chinese-CLIP on the COCO-CN *all* set, both using ViT-B-based models, for text-to-image retrieval.

splits		the <i>test</i> set				the <i>all</i> set			
metric		R@1	R@5	R@10	mR	R@1	R@5	R@10	mR
vanilla		62.12	86.62	92.52	80.42	24.35	44.78	54.36	41.16
GA	CO	65.60	89.04	94.18	82.94	26.79	48.20	57.91	44.30
	F30k	66.00	89.40	94.44	83.28	27.59	49.16	58.79	45.18
BP	CO	66.58	89.28	94.36	83.41	27.68	49.51	59.17	45.45
	F30k	67.18	89.92	94.56	83.89	27.99	49.81	59.49	45.76

Table 11. Flickr30k-CNA text-to-image retrieval results based on ViT-B. CO indicates that AAT is optimized on the COCO-CN *val* set, while F30k indicates optimization on a 1k-sample subset of the Flickr30k-CNA *val* set.

tasks	ACT	CEL	COL	CNT	FIG	OBJ	OCR	POS	SCE	mean
$\mathcal{S}_{\text{gain}}$	2.26	2.91	2.02	2.59	2.29	2.84	3.79	2.34	2.40	2.60
$\mathcal{S}_{\text{loss}}$	2.60	3.87	2.74	2.77	2.72	3.05	4.03	2.74	3.25	3.09

Table 12. Average text-related importance of ablated heads in the last 4 layers on natural ReCoS (reported values in units of $1e-2$).

requiring no gradients, it is roughly $20\times$ slower than BP due to a vast number of fitness evaluations, even with a small \mathcal{D} .

AAT is designed as an “out-of-the-box” solution where GA hyper-parameters (*e.g.*, generations, crossover/mutation rates) are kept fixed across model sizes to minimize manual adjustment. This simplicity introduces redundant overhead. We therefore apply the following practical optimizations:

1. **Skipping:** Based on the analysis in Appendix 9, where effective ablation ratios typically fall between 30% and 40%, we skip candidates whose ratios exceed 60%.
2. **Reducing population size for ViT-L/H:** We find that the reduced population sizes maintain comparable accuracy while significantly cutting runtime.
3. **Fewer generations:** We find that performance plateaus in the final 30% of generations, despite a continued fitness gain, suggesting that over-optimization on \mathcal{D} offers diminishing benefit on test data.

These adjustments yield substantial overhead savings—reducing GA runtime by 40%, 70%, and 72% for the base, large, and huge models, with only minor performance drops (Table 13; detailed comparisons in Appendix 10). As post-training technique, both AAT-BP and AAT-GA impose minimal cost compared to training CLIP from scratch, underscoring their practicality for real-world deployment.

5.6. An Interpretability Perspective on AAT

We investigate the interpretability of the ablated heads using TextSpan [11] to correlate head-level effects to linguistic

size	metric	vanilla	BP	GA	GA (opt)
B	mR	58.9	60.9	61.5	61.2
	runtime	-	2 min (0.3 GHs)	30 min (4 GHs)	18 min (2.4 GHs)
L	mR	63.7	66.2	66.1	65.9
	runtime	-	5 min (0.7 GHs)	1.5 h (12 GHs)	27 min (3.6 GHs)
H	mR	66.8	68.1	68.7	68.3
	runtime	-	8 min (1.1 GHs)	3 h (24 GHs)	50 min (6.7 GHs)

Table 13. Mean-R on MS COCO *test* set for text-to-image retrieval vs. actual optimization runtime. “Opt” denotes AAT-GA with optimized hyper-parameter settings; “GHs” denotes the GPU hours.

semantics. Using a ViT-B-based CLIP model, for each image–text pair we extract the text and image embeddings and, following TextSpan, decompose the image embedding into 144 (12×12) head-specific image embeddings. Each one is then multiplied by the text embedding to yield a 12×12 matrix of text-related importance, where larger values indicate higher semantic relevance. This matrix reveals which heads in vanilla CLIP are most (or least) aligned with the text.

We probe these semantics on the natural subsets of ReCoS. Specifically, we partition all natural pairs into those that flip from incorrect to correct after applying AAT-GA ($\mathcal{S}_{\text{gain}}$) and those that flip from correct to incorrect ($\mathcal{S}_{\text{loss}}$). For each pair, we compute the cumulative text-related importance (from the 12×12 matrix) of the heads ablated by AAT in the last four layers, as recommended by TextSpan. As shown in Table 12, the ablated heads in $\mathcal{S}_{\text{gain}}$ have lower average importance, whereas those in $\mathcal{S}_{\text{loss}}$ have higher importance. This supports the view that suppressing less text-relevant heads tends to improve image–text alignment (and suppressing highly text-relevant heads can harm it) [11].

These findings complement the CLIP interpretability research [11], which manually removes heads associated with spurious cues in specific layers and observes improved representations. Instead, AAT offers an automated, data-driven scheme that can target detrimental heads across all layers. Encouragingly, AAT naturally focuses on heads with lower text-related importance, echoing those manual intervention results. It thereby reinforces the conclusion that attention heads exhibit meaningful semantic structure.

6. Conclusion

To better understand CLIP’s attention mechanism, we conduct comprehensive analysis of attention heads in its image encoder. Observing heterogeneous head impacts, we propose AAT, a simple but effective method that refines representations by systematically ablating detrimental heads via attention-weight manipulation. For detrimental head identification, we present two alternative strategies: AAT-GA that suited to limited floating-point compute (*e.g.*, INT8/INT16 edge devices), and AAT-BP which offers greater optimiza-

tion efficiency when resources allow. Experimental results demonstrate that AAT improves CLIP-family models across diverse downstream tasks, achieves far greater parameter efficiency than PEFT, and corroborates recent interpretability findings. We hope this study contributes to deeper understanding of CLIP and paves the way to efficiency of VLMs.

References

- [1] Reza Abbasi, Mohammad Hossein Rohban, and Mahdieh Soleymani Baghshah. Deciphering the role of representation disentanglement: Investigating compositional generalization in clip models. In *European Conference on Computer Vision*, pages 35–50. Springer, 2025. 1
- [2] Maximiliana Behnke and Kenneth Heafield. Losing heads in the lottery: Pruning transformer. In *The 2020 Conference on Empirical Methods in Natural Language Processing*, pages 2664–2674. Association for Computational Linguistics (ACL), 2020. 2
- [3] Usha Bhalla, Alex Oesterling, Suraj Srinivas, Flavio P Calmon, and Himabindu Lakkaraju. Interpreting clip with sparse linear concept embeddings (splice). *arXiv preprint arXiv:2402.10376*, 2024. 2
- [4] Gianni Brauwers and Flavius Frasincar. A general survey on attention mechanisms in deep learning. *IEEE Transactions on Knowledge and Data Engineering*, 35(4):3279–3298, 2021. 2
- [5] Xiaojun Chen, Jimeng Lou, Wenxi Huang, Ting Wan, Qin Zhang, and Min Yang. Recos: A novel benchmark for cross-modal image-text retrieval in complex real-life scenarios. In *Proceedings of the 32nd ACM International Conference on Multimedia*, pages 9165–9174, 2024. 5
- [6] Jaemin Cho, Jie Lei, Hao Tan, and Mohit Bansal. Unifying vision-and-language tasks via text generation. In *International Conference on Machine Learning*, pages 1931–1942. PMLR, 2021. 1
- [7] Jonathan Crabbé, Pau Rodriguez, Vaishaal Shankar, Luca Zappella, and Arno Blaas. Interpreting clip: Insights on the robustness to imagenet distribution shifts. *Transactions on Machine Learning Research*, 2024. 2
- [8] Jia Deng, Wei Dong, Richard Socher, Li-Jia Li, Kai Li, and Li Fei-Fei. Imagenet: A large-scale hierarchical image database. In *2009 IEEE conference on computer vision and pattern recognition*, pages 248–255. Ieee, 2009. 5
- [9] Ning Ding, Yujia Qin, Guang Yang, Fuchao Wei, Zonghan Yang, Yusheng Su, Shengding Hu, Yulin Chen, Chi-Min Chan, Weize Chen, et al. Parameter-efficient fine-tuning of large-scale pre-trained language models. *Nature Machine Intelligence*, 5(3):220–235, 2023. 2
- [10] Alexey Dosovitskiy. An image is worth 16x16 words: Transformers for image recognition at scale. *arXiv preprint arXiv:2010.11929*, 2020. 3
- [11] Yossi Gandelsman, Alexei A Efros, and Jacob Steinhardt. Interpreting clip’s image representation via text-based decomposition. In *The Twelfth International Conference on Learning Representations*, 2024. 1, 2, 8
- [12] John H Holland. *Adaptation in natural and artificial systems: an introductory analysis with applications to biology, control, and artificial intelligence*. MIT press, 1992. 3
- [13] Neil Houlsby, Andrei Giurgiu, Stanislaw Jastrzebski, Bruna Morrone, Quentin De Laroussilhe, Andrea Gesmundo, Mona Attariyan, and Sylvain Gelly. Parameter-efficient transfer learning for nlp. In *International conference on machine learning*, pages 2790–2799. PMLR, 2019. 2, 4
- [14] Edward J Hu, Phillip Wallis, Zeyuan Allen-Zhu, Yuanzhi Li, Shean Wang, Lu Wang, Weizhu Chen, et al. Lora: Low-rank adaptation of large language models. In *International Conference on Learning Representations*, 2022. 2, 4
- [15] Gabriel Ilharco, Mitchell Wortsman, Ross Wightman, Cade Gordon, Nicholas Carlini, Rohan Taori, Achal Dave, Vaishaal Shankar, Hongseok Namkoong, John Miller, Hananeh Hajishirzi, Ali Farhadi, and Ludwig Schmidt. Openclip, 2021. 4, 3
- [16] Chao Jia, Yinfei Yang, Ye Xia, Yi-Ting Chen, Zarana Parekh, Hieu Pham, Quoc Le, Yun-Hsuan Sung, Zhen Li, and Tom Duerig. Scaling up visual and vision-language representation learning with noisy text supervision. In *International conference on machine learning*, pages 4904–4916. PMLR, 2021. 1
- [17] Eunji Kim, Kyuhong Shim, Simyung Chang, and Sungroh Yoon. Semantic token reweighting for interpretable and controllable text embeddings in clip. In *Findings of the Association for Computational Linguistics: EMNLP 2024*, pages 14330–14345, 2024. 2
- [18] Mengcheng Lan, Chaofeng Chen, Yiping Ke, Xinjiang Wang, Litong Feng, and Wayne Zhang. Clearclip: Decomposing clip representations for dense vision-language inference. In *European Conference on Computer Vision*, pages 143–160. Springer, 2025. 1, 2
- [19] Brian Lester, Rami Al-Rfou, and Noah Constant. The power of scale for parameter-efficient prompt tuning. In *Proceedings of the 2021 Conference on Empirical Methods in Natural Language Processing*. Association for Computational Linguistics, 2021. 2
- [20] Junnan Li, Ramprasaath Selvaraju, Akhilesh Gotmare, Shafiq Joty, Caiming Xiong, and Steven Chu Hong Hoi. Align before fuse: Vision and language representation learning with momentum distillation. *Advances in neural information processing systems*, 34:9694–9705, 2021. 1
- [21] Xirong Li, Chaoxi Xu, Xiaoxu Wang, Weiyu Lan, Zhengxiong Jia, Gang Yang, and Jieping Xu. Coco-cn for cross-lingual image tagging, captioning, and retrieval. *IEEE Transactions on Multimedia*, 21(9):2347–2360, 2019. 2, 5
- [22] Yi Li, Hualiang Wang, Yiqun Duan, and Xiaomeng Li. Clip surgery for better explainability with enhancement in open-vocabulary tasks. *arXiv preprint arXiv:2304.05653*, 2023. 2
- [23] Tsung-Yi Lin, Michael Maire, Serge Belongie, James Hays, Pietro Perona, Deva Ramanan, Piotr Dollár, and C Lawrence Zitnick. Microsoft coco: Common objects in context. In *Computer Vision—ECCV 2014: 13th European Conference, Zurich, Switzerland, September 6–12, 2014, Proceedings, Part V 13*, pages 740–755. Springer, 2014. 5

- [24] Shi Liu, Kecheng Zheng, and Wei Chen. Paying more attention to image: A training-free method for alleviating hallucination in lvlms. In *European Conference on Computer Vision*, pages 125–140. Springer, 2025. 2
- [25] Timo Lüddecke and Alexander Ecker. Image segmentation using text and image prompts. In *Proceedings of the IEEE/CVF conference on computer vision and pattern recognition*, pages 7086–7096, 2022. 1
- [26] Joanna Materzyńska, Antonio Torralba, and David Bau. Disentangling visual and written concepts in clip. In *Proceedings of the IEEE/CVF Conference on Computer Vision and Pattern Recognition*, pages 16410–16419, 2022. 2
- [27] Paul Michel, Omer Levy, and Graham Neubig. Are sixteen heads really better than one? *Advances in neural information processing systems*, 32, 2019. 2
- [28] Alec Radford, Jong Wook Kim, Chris Hallacy, Aditya Ramesh, Gabriel Goh, Sandhini Agarwal, Girish Sastry, Amanda Askell, Pamela Mishkin, Jack Clark, et al. Learning transferable visual models from natural language supervision. In *International conference on machine learning*, pages 8748–8763. PMLR, 2021. 1, 4
- [29] Arijit Ray, Filip Radenovic, Abhimanyu Dubey, Bryan Plummer, Ranjay Krishna, and Kate Saenko. Cola: A benchmark for compositional text-to-image retrieval. *Advances in Neural Information Processing Systems*, 36, 2024. 1
- [30] Christoph Schuhmann, Romain Beaumont, Richard Vencu, Cade Gordon, Ross Wightman, Mehdi Cherti, Theo Coombes, Aarush Katta, Clayton Mullis, Mitchell Wortsman, et al. Laion-5b: An open large-scale dataset for training next generation image-text models. *Advances in Neural Information Processing Systems*, 35:25278–25294, 2022. 4
- [31] Peiyang Shi, Michael C Welle, Márten Björkman, and Danica Kragic. Towards understanding the modality gap in clip. In *ICLR 2023 Workshop on Multimodal Representation Learning: Perks and Pitfalls*, 2023. 2
- [32] Yi-Lin Sung, Jaemin Cho, and Mohit Bansal. Lst: Ladder side-tuning for parameter and memory efficient transfer learning. *Advances in Neural Information Processing Systems*, 35:12991–13005, 2022. 2
- [33] Elena Voita, David Talbot, Fedor Moiseev, Rico Sennrich, and Ivan Titov. Analyzing multi-head self-attention: Specialized heads do the heavy lifting, the rest can be pruned. In *Proceedings of the 57th Annual Meeting of the Association for Computational Linguistics*, pages 5797–5808, 2019. 2
- [34] Zhengxuan Wu, Aryaman Arora, Zheng Wang, Atticus Geiger, Dan Jurafsky, Christopher D Manning, and Christopher Potts. Reft: representation finetuning for language models. In *Proceedings of the 38th International Conference on Neural Information Processing Systems*, pages 63908–63962, 2024. 2, 5
- [35] Chunyu Xie, Heng Cai, Jincheng Li, Fanjing Kong, Xiaoyu Wu, Jianfei Song, Henrique Morimitsu, Lin Yao, Dexin Wang, Xiangzheng Zhang, et al. Ccmb: A large-scale chinese cross-modal benchmark. In *Proceedings of the 31st ACM International Conference on Multimedia*, pages 4219–4227, 2023. 5
- [36] An Yang, Junshu Pan, Junyang Lin, Rui Men, Yichang Zhang, Jingren Zhou, and Chang Zhou. Chinese clip: Contrastive vision-language pretraining in chinese. *arXiv preprint arXiv:2211.01335*, 2022. 2, 4
- [37] Peter Young, Alice Lai, Micah Hodosh, and Julia Hockenmaier. From image descriptions to visual denotations: New similarity metrics for semantic inference over event descriptions. *Transactions of the Association for Computational Linguistics*, 2:67–78, 2014. 5
- [38] Zhongzhi Yu, Zheng Wang, Yonggan Fu, Huihong Shi, Khalid Shaikh, and Yingyan Celine Lin. Unveiling and harnessing hidden attention sinks: Enhancing large language models without training through attention calibration. In *International Conference on Machine Learning*, 2024. 2
- [39] Maxime Zanella and Ismail Ben Ayed. Low-rank few-shot adaptation of vision-language models. In *Proceedings of the IEEE/CVF Conference on Computer Vision and Pattern Recognition*, pages 1593–1603, 2024. 5
- [40] Xiaohua Zhai, Basil Mustafa, Alexander Kolesnikov, and Lucas Beyer. Sigmoid loss for language image pre-training. In *Proceedings of the IEEE/CVF International Conference on Computer Vision*, pages 11975–11986, 2023. 1
- [41] Chenyang Zhao, Kun Wang, Xingyu Zeng, Rui Zhao, and Antoni B Chan. Gradient-based visual explanation for transformer-based clip. In *International Conference on Machine Learning*, pages 61072–61091. PMLR, 2024. 2
- [42] Kaiyang Zhou, Jingkang Yang, Chen Change Loy, and Ziwei Liu. Conditional prompt learning for vision-language models. In *Proceedings of the IEEE/CVF conference on computer vision and pattern recognition*, pages 16816–16825, 2022. 1

Not All Attention Heads Are What You Need: Refining CLIP’s Image Representation with Attention Ablation

Supplementary Material

7. Benchmark Details and Evaluation Metrics

7.1. MS COCO

MS COCO is a large-scale dataset with 91 object categories in natural contexts, comprising about 113,287 training, 5,000 validation, and 5,000 test images (with annotations not publicly available), annotated with bounding boxes, segmentation, and 5 descriptive texts per image. For our experiments, we reconstruct the available training and validation images into two test sets: the *test* set, which corresponds to the original validation set, and the *all* set, which includes both the training and validation images. We evaluate MS COCO for text-to-image and image-to-text retrieval using recall rates at k ($R@1$, $R@5$, $R@10$) and mean-R (the average of $R@1$, $R@5$, and $R@10$) as the evaluation metrics.

7.2. Flickr30k

Flickr30k contains 31k images collected from Flickr, each accompanied by 5 reference sentences provided by human annotators. The dataset is split into 29k training images, 1k validation images, and 1k test images. Similarly to MS COCO, we treat the test images as the *test* set and the entire dataset as the *all* set. Both reconstructed sets are used to evaluate our method for text-to-image and image-to-text retrieval, with recall rates as the evaluation metric.

7.3. ReCoS

ReCoS is a benchmark designed for image-text retrieval in real-world scenarios, comprising 12 overlapping subsets with a total of 1k test images and diverse annotations per subset. We follow the standardized ReCoS-v1 evaluation protocol for experiments and report $R@1$ performance for text-to-image retrieval across all 12 subsets, as done in the original ReCoS paper. The subset abbreviations in Table 5 are: ACT for *action*, CEL for *celebrity*, COL for *color*, CNT for *count*, FIG for *figure*, OBJ for *object*, POS for *position*, SCE for *scene*, CR for *code reasoning*, NC for *numerical calculation*, and TT for *text translation*.

7.4. COCO-CN

COCO-CN is a Chinese image-text retrieval dataset with about 18k training, 1k validation, and 1k test images, annotated with 27,218 manually written Chinese sentences. In our experiments, we use the COCO-CN test images as the *test* set and all images as the *all* set, evaluating both sets with the same metric used for MS COCO.

7.5. Flickr30k-CNA

Flickr30k-CNA is a cleaned Chinese-translated version of Flickr30k, with captions generated by professional English–Chinese linguists. We process and evaluate it following the same protocol used for Flickr30k.

7.6. ImageNet-1k

ImageNet-1k is a widely used image classification benchmark originally curated for the Large Scale Visual Recognition Challenge (ILSVRC). It contains 1k object categories, with over 1.2 million labeled training images, 50,000 validation images, and 100,000 test images. ImageNet-1k also serves as a standard benchmark for zero-shot classification. During inference, object class names (provided in the CLIP repository¹) are converted into textual prompts using several predefined templates². In our experiments, we evaluate zero-shot classification performance on the ImageNet-1k *val* set using top-1 accuracy as the metric.

7.7. Cola

Cola [29] is a compositional text-to-image retrieval benchmark designed to evaluate a model’s ability to localize and compose objects with their corresponding attributes. It includes both real-world images and synthetic 3D-rendered scenes. The task requires retrieving images that match the correct configuration of objects and attributes while rejecting distractors that contain the right components in incorrect arrangements. *Cola* consists of approximately 1.2k composed queries involving 168 objects and 197 attributes, distributed across roughly 30K images. It features two types of queries: single-object compositions (sourced from GQA, CLEVR, and PACO) and multi-object queries. Following the original paper, mean average precision (mAP) is used for evaluating single-object subsets, while mean accuracy is used for the multi-object subset.

8. Impact of Individual Attention Heads

As described in Section 3, we investigate the impact of each individual attention head in CLIP’s image encoder on text-to-image retrieval performance. Detailed results are provided in Table 19. As shown, ablating even a single attention head can outperform the vanilla baseline, reaching

¹https://github.com/OFA-Sys/Chinese-CLIP/blob/master/zeroshot_dataset_en.md

²https://github.com/LAION-AI/CLIP_benchmark/blob/main/clip_benchmark/datasets/en_zeroshot_classification_templates.json

tasks		text-to-image retrieval								image-to-text retrieval							
splits		the <i>test</i> set				the <i>all</i> set				the <i>test</i> set				the <i>all</i> set			
size	method	R@1	R@5	R@10	mR	R@1	R@5	R@10	mR	R@1	R@5	R@10	mR	R@1	R@5	R@10	mR
B	vanilla	62.2	86.9	94.3	81.1	24.0	45.4	55.8	41.7	56.2	83.8	93.4	77.8	22.6	43.0	52.7	39.4
	naive h-a	62.7	89.6	95.6	82.6	25.2	47.0	57.5	43.2	55.8	85.5	93.4	78.2	23.6	45.0	55.0	41.2
L	vanilla	63.9	88.7	94.5	82.4	26.7	48.6	58.5	44.6	60.4	84.2	93.3	79.3	24.4	44.6	54.5	41.2
	naive h-a	65.9	89.9	95.6	83.8	28.9	51.2	61.4	47.2	61.6	86.1	93.8	80.5	27.7	47.9	59.2	44.9
H	vanilla	69.6	89.9	95.8	85.1	30.4	52.4	62.2	48.3	63.1	86.7	93.0	80.9	26.3	46.5	56.0	42.9
	naive h-a	71.8	91.3	97.0	86.7	32.6	55.0	64.9	50.8	64.2	87.7	94.2	82.0	28.5	48.7	59.4	45.5

Table 14. Comparison on COCO-CN for retrieval. R@k denotes recall at rank k, and mR (mean-R) is the average of R@1, R@5, and R@10. Model sizes are denoted as B (ViT-B), L (ViT-L), and H (ViT-H). “Vanilla” refers to the baseline model, while “naive h-a” indicates the model enhanced via naive joint head ablation.

up to 81.1% mean-R. Conversely, removing certain critical heads leads to a significant performance drop of up to 3.7% compared to the baseline. These results highlight the distinct roles of individual heads and suggest that carefully selecting which heads to ablate could yield further performance gains.

In the main content of the paper, we identify all negatively impactful heads—those that individually yield higher retrieval performance than the vanilla baseline when ablated—and jointly ablate them in a simple strategy referred to as naive joint head ablation (naive h-a). We extend this experiment across different model sizes for both text-to-image and image-to-text retrieval on COCO-CN. As shown in Table 14, even this straightforward method surpasses the baseline by 1.4%~1.6% on the *test* set and 1.5%~2.6% on the *all* set for text-to-image retrieval, and by 0.4%~1.2% on the *test* set and 1.8%~3.7% on the *all* set for image-to-text retrieval.

9. Analysis of the Ablated Heads

9.1. Layer Distribution

To illustrate the effect of AAT, we present the distribution of ablated heads in AAT-GA across layers for ViT-B, ViT-L, and ViT-H-based models in Figure 4, covering both English and Chinese versions of CLIP. The results reveal that CLIP models tend to have greater head redundancy (*i.e.*, more detrimental heads) in the shallow and deep layers, with fewer in the intermediate layers. In contrast, Chinese-CLIP models exhibit a more balanced ablation pattern across all layers.

9.2. Statistics

We report the overall ablation ratio (calculated as the number of ablated heads divided by the total number of heads) and the average number of ablated heads per layer for different model sizes in Table 15. As shown, both CLIP and Chinese-CLIP models follow similar trends: base models have ablation ratios around 0.3, while larger models reach

model	metric	ViT-B	ViT-L	ViT-H
CLIP	ratio	0.31	0.34	0.40
	avg	3.7	5.4	6.4
Chinese-CLIP	ratio	0.28	0.38	0.40
	avg	3.4	6.1	6.4

Table 15. Overall ablation ratio and average ablated heads per layer across different model sizes and languages. The results are averaged over three AAT-GA runs with different random seeds.

up to 0.4. This supports the intuition that larger models contain more redundant attention heads.

10. Computational Cost Analysis

We optimize AAT-GA by eliminating redundant overhead, as described in Section 5.5 of the paper. Detailed performance and runtime comparisons under different hyper-parameter configurations are provided in Tables 16 and 17.

Table 16 reports AAT-GA performance and optimization runtime across various hyper-parameter settings. Based on these results, we identify efficient GA configurations: `gen = 75` and `psize = 48` for ViT-B/L models, and `gen = 75` and `psize = 64` for ViT-H models. As shown in Table 17, skipping fitness evaluations for high-ablation-ratio candidates further improves efficiency compared to the unified configuration. The final runtime cost and corresponding performance are summarized in Table 13 in the main paper.

11. Evaluation on Compositional Retrieval

Compositional retrieval is a challenging task that goes beyond conventional cross-modal retrieval by requiring a deeper understanding of object relationships, attributes, and reasoning—rather than relying solely on visual perception. In order to explore the potential of AAT in this setting, we evaluate AAT-improved CLIP on *Cola*, a recently proposed challenging benchmark designed for compositional text-to-image retrieval across both real-world and synthetic domains.

	single-object			multi-object
	GQA	CLEVR	PACO	
vanilla	35.36	7.57	26.38	18.10
AAT-GA	37.63	7.54	28.33	20.48
AAT-BP	36.41	7.27	27.69	21.90

Table 18. Comparison of CLIP and AAT-improved CLIP on *Cola*. Results are based on ViT-B, with mAP used as evaluation metric for single-object queries and mean accuracy for multi-object queries.

due to overfitting or convergence to local minima under limited data. This instability is consistent across repeated trials, highlighting the challenges of SFT in data-scarce settings.

Although SFT beats AAT in some cases, AAT exhibits markedly stronger cross-domain generalization. As shown in the right column of Figure 5, AAT consistently outperforms SFT by at least 1.27% on ViT-B, 0.06% on ViT-L, and 1.37% on ViT-H. Notably, the SFT models that perform best on COCO-CN exhibit substantial performance degradation on Flickr30k-CNA, in some cases even falling below the baseline. This indicates a vulnerability of SFT when trained on limited data.

13. Visualization

13.1. AAT Optimization Data

For the convenience of readers, we provide a visualization of the validation set \mathcal{D} used for AAT optimization in Figure 6.

13.2. Failure Cases

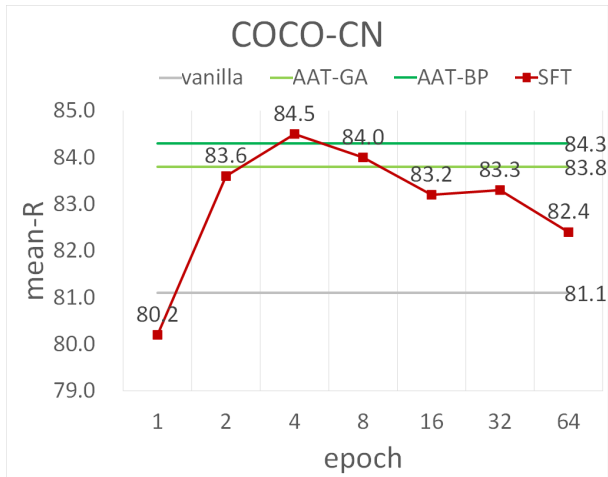
As discussed in Appendix 11 and Section 5.2.1 of the paper, AAT fails on *Cola*-CLEVR and three non-natural subsets from ReCoS. Representative examples from these tasks are shown in Figure 7 and Figure 8, respectively. As illustrated, there exists a significant domain gap between the test images and those in \mathcal{D} . Moreover, certain tasks require models to perform high-level comprehension and reasoning, which exceeds the representational capacity of CLIP.

14. Limitations

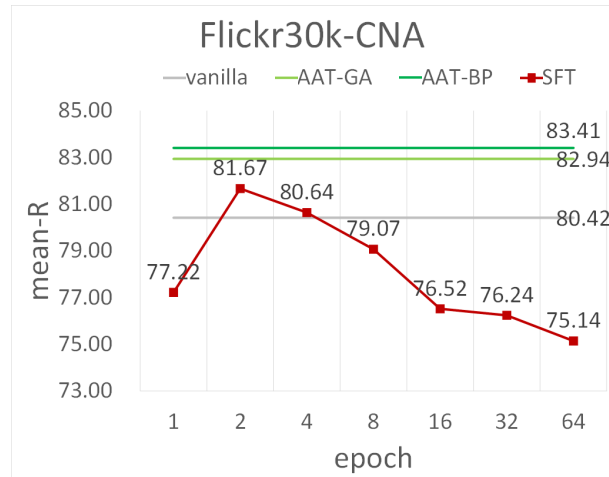
We summarize four limitations of this work, which we leave as directions for future exploration:

- **Sample Selection for Optimization:** It remains unclear how to optimally select the samples used for AAT optimization—specifically, which image-text pairs are most effective for refining the output representations while ensuring broad generalization.
- **Dependence on Optimization Data:** Although AAT is designed for data-scarce scenarios, it still requires a small validation set. Head selection is inherently data-dependent, even when the dataset is indeed minimal.

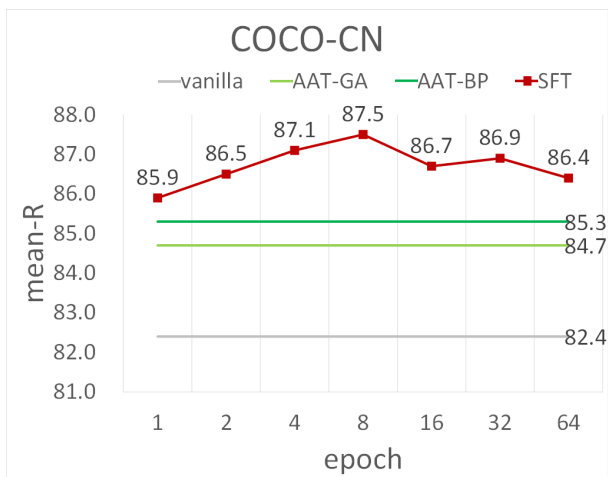
- **Limited Validation on More Challenging Tasks:** AAT has not yet been evaluated on downstream tasks beyond cross-modal alignment, such as visual question answering (VQA), object detection, or semantic segmentation. Its applicability to these more complex settings remains an open question.
- **Lack of Per-Instance Adaptation:** AAT performs ablation globally based on the entire validation set, without per-instance customization. In practice, certain attention heads may be detrimental in some contexts but beneficial in others. This suggests a promising direction: per-image adaptive head ablation, where head selection is dynamically tailored to the input characteristics.



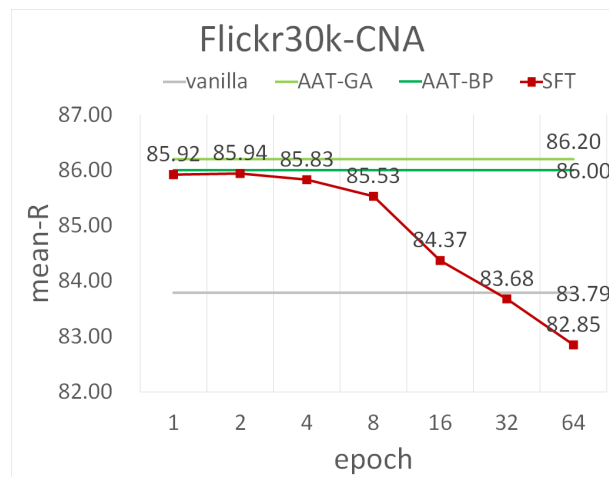
(a) Mean-R on COCO-CN, based on ViT-B.



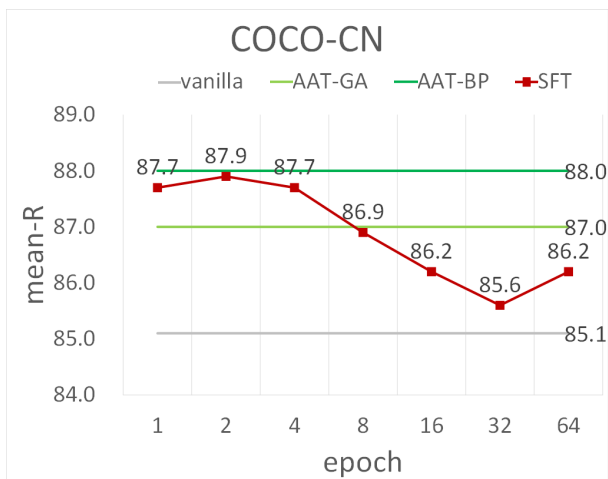
(b) Mean-R on Flickr30k-CNA, based on ViT-B.



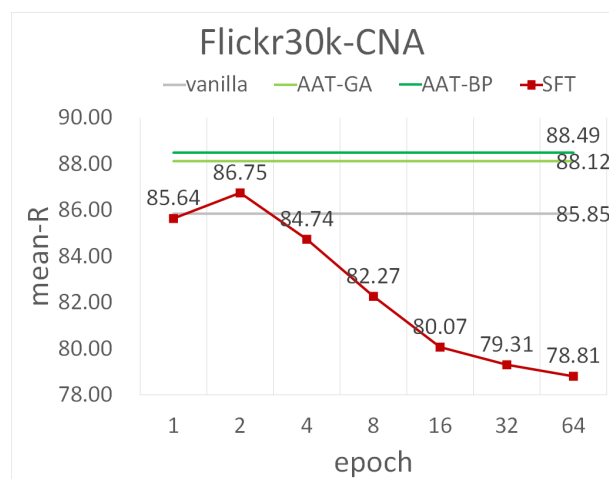
(c) Mean-R on COCO-CN, based on ViT-L.



(d) Mean-R on Flickr30k-CNA, based on ViT-L.



(e) Mean-R on COCO-CN, based on ViT-H.



(f) Mean-R on Flickr30k-CNA, based on ViT-H.

Figure 5. Comparison for text-to-image retrieval among AAT-improved models, the SFT models, and the vanilla counterparts. For SFT models, mean-R across increasing training epochs are reported. Evaluation is conducted on the *test* sets of COCO-CN and Flickr30k-CNA for each model variant.



Figure 6. Visualization of samples from the validation set \mathcal{D} used for AAT optimization, sourced from MS COCO. Each image is paired with a single text description, such as, “An old woman sits next to a large stuffed teddy bear on a bench,” which corresponds to first image in the top row.

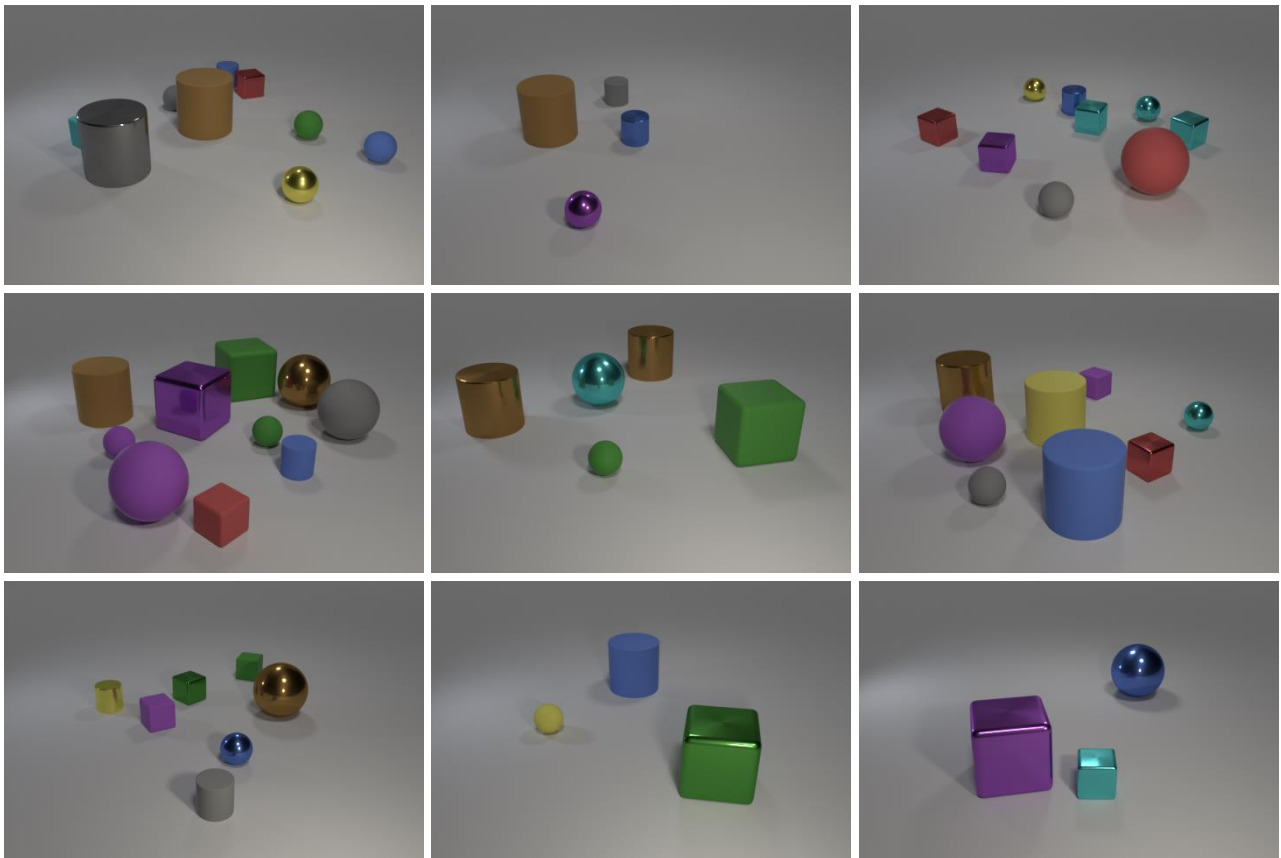
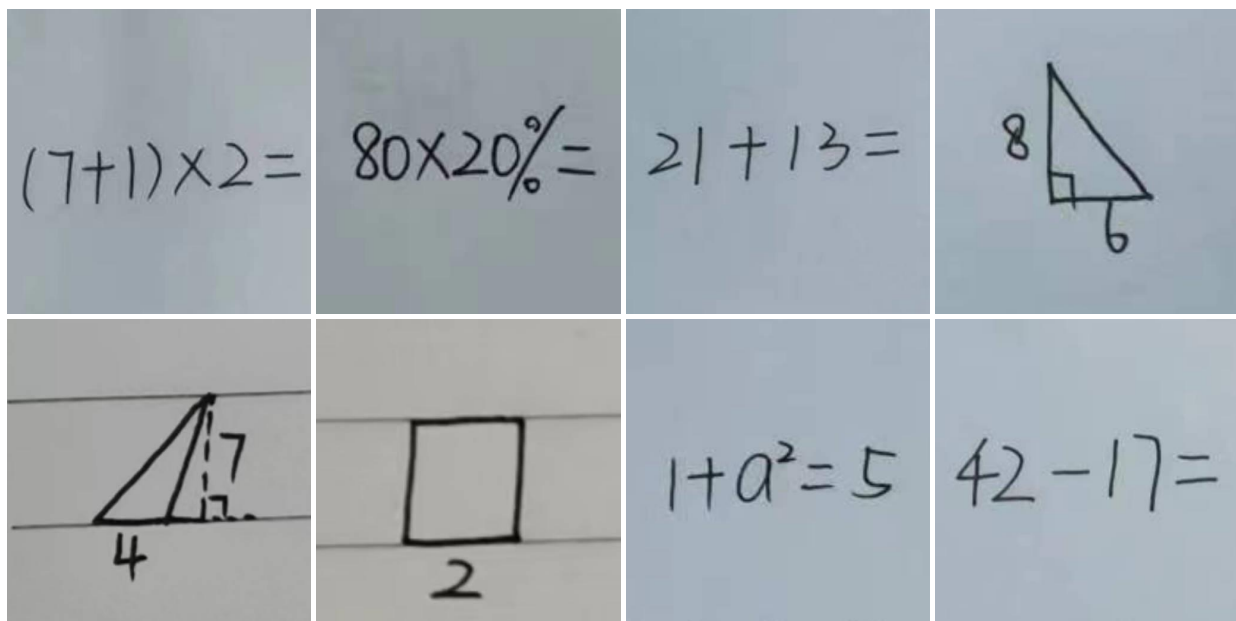


Figure 7. Visualization of samples from *Cola*-CLEVR, a subset of *Cola* used as a retrieval benchmark in this paper. Each image is paired with a set of descriptive attributes, such as “large,” “purple,” “rubber,” “cube,” “metal,” etc.

<pre>x = 5 y = 2 z = x + y print(z)</pre>	<pre>for i in range(5): for j in range(2): print(j)</pre>	<pre>import numpy as np result = np.sqrt(125) print(result)</pre>	<pre>x = 5 y = 10 x = x ^ y y = x ^ y x = x ^ y print(f"x: {x}, y: {y}")</pre>
<pre>def add(x, y): return x * y result = add(3, 4) print(result)</pre>	<pre>msg = "Python" substring = msg[2:] print(substring)</pre>	<pre>a_name = "John" b_name = "Doe" name = a_name + "-" + b_name print(name)</pre>	<pre>matrix = [[1, 2, 3], [4, 5, 6], [7, 8, 9]] for row in matrix: for num in row: num += 1 print(num)</pre>

(a) Illustrative examples from the subset of code reasoning within ReCoS-v1. Each image is paired with a text description explaining the reasoning process behind the code presented in the image.



(b) Illustrative examples from the subset of numerical calculation within ReCoS-v1. Each image is paired with a text description that either provides answers to numerical calculations or describes the geometric shapes depicted in the image.

美味的晚餐	北京故宫	丰盛的午餐	脆皮烤鸭
美丽的上海	有点困	棕色的狗	我去运动了

(c) Illustrative examples from the subset of text translation within ReCoS-v1. Each image is paired with a text description that provides the English translation of the Chinese text depicted in the image. For instance, "The English translation corresponding to the text in the text-only picture is 'Delicious dinner,'" corresponds to the first image in the top row.

Figure 8. Visualization of non-natural images from three ReCoS-v1 subsets: code reasoning (CR), numerical calculation (NC), and text translation (TT).

l	h	R@1	R@5	R@10	mR	l	h	R@1	R@5	R@10	mR	l	h	R@1	R@5	R@10	mR
0	0	60.8	86.0	93.5	80.1	1	0	60.3	86.3	93.7	80.1	2	0	60.8	86.3	93.3	80.1
	1	59.9	86.3	93.4	79.9		1	60.7	86.2	93.2	80.0		1	60.4	86.1	93.2	79.9
	2	60.4	86.2	93.2	79.9		2	60.9	86.4	93.0	80.1		2	60.1	86.3	93.2	79.9
	3	60.2	86.5	93.3	80.0		3	60.6	85.7	93.3	79.9		3	60.1	85.9	93.3	79.8
	4	60.8	86.3	93.5	80.2		4	60.2	85.8	93.4	79.8		4	60.3	86.0	93.3	79.9
	5	60.2	86.3	93.3	79.9		5	60.3	86.1	93.2	79.9		5	60.7	85.9	93.2	79.9
	6	60.5	86.1	93.4	80.0		6	60.4	86.2	93.2	79.9		6	60.3	85.8	93.4	79.8
	7	60.0	86.2	93.6	79.9		7	60.2	86.4	93.2	79.9		7	58.2	85.1	93.0	78.8
	8	60.4	86.4	93.2	80.0		8	60.4	86.3	93.3	80.0		8	60.4	86.6	93.1	80.0
	9	60.3	86.2	93.2	79.9		9	60.6	86.3	93.2	80.0		9	60.5	86.1	93.2	79.9
	10	60.4	86.4	93.2	80.0		10	60.2	86.1	93.4	79.9		10	60.3	86.3	93.4	80.0
11	60.2	85.9	93.6	79.9	11	60.4	86.0	93.2	79.9	11	60.7	86.5	93.0	80.1			
3	0	60.9	85.7	93.6	80.1	4	0	60.6	86.4	93.4	80.1	5	0	60.8	85.8	93.4	80.0
	1	60.1	86.1	93.1	79.8		1	59.3	85.9	93.2	79.5		1	60.4	86.2	93.4	80.0
	2	59.1	85.8	92.6	79.2		2	60.4	85.8	93.2	79.8		2	60.6	86.1	93.4	80.0
	3	60.0	86.2	93.3	79.8		3	60.0	86.4	93.1	79.8		3	58.9	84.4	92.4	78.6
	4	59.6	85.9	93.4	79.6		4	60.2	85.8	93.4	79.8		4	60.6	86.5	93.3	80.1
	5	60.3	86.6	93.1	80.0		5	59.9	86.3	93.3	79.8		5	60.2	86.0	93.3	79.8
	6	60.5	86.3	93.2	80.0		6	59.7	86.4	93.3	79.8		6	59.9	86.2	93.3	79.8
	7	60.5	86.3	93.4	80.1		7	61.1	86.0	93.3	80.1		7	60.6	86.4	93.6	80.2
	8	60.7	86.5	93.3	80.2		8	60.4	86.4	93.4	80.1		8	60.1	85.7	93.4	79.7
	9	60.1	86.5	93.3	80.0		9	59.1	85.9	93.2	79.4		9	60.3	86.5	93.1	80.0
	10	59.7	86.8	93.2	79.9		10	60.3	86.4	93.5	80.1		10	60.0	85.4	93.1	79.5
11	57.4	83.3	91.0	77.2	11	60.2	86.1	92.9	79.7	11	61.0	86.0	93.5	80.2			
6	0	60.4	86.3	93.1	79.9	7	0	60.0	85.8	93.4	79.7	8	0	60.4	86.5	93.3	80.1
	1	59.4	86.2	93.4	79.7		1	60.1	86.2	93.3	79.9		1	59.8	86.0	92.9	79.6
	2	59.9	85.3	92.9	79.4		2	61.0	86.7	93.3	80.3		2	55.0	83.7	91.2	76.6
	3	60.4	86.2	93.1	79.9		3	59.3	86.0	92.8	79.4		3	60.5	86.1	93.4	80.0
	4	60.6	86.3	93.4	80.1		4	60.2	86.2	92.9	79.8		4	79.9	85.9	93.3	79.9
	5	59.9	86.4	93.2	79.8		5	60.5	86.2	93.3	80.0		5	60.3	86.2	93.4	80.0
	6	59.5	86.3	93.4	79.7		6	59.9	86.2	92.9	79.7		6	60.7	85.7	92.8	79.7
	7	60.3	86.2	93.1	79.9		7	60.3	86.5	93.1	80.0		7	60.4	86.4	93.0	79.9
	8	60.3	86.1	93.5	80.0		8	60.6	86.2	93.2	80.0		8	60.0	86.7	92.8	79.8
	9	60.7	86.2	93.2	80.0		9	60.1	85.9	93.1	79.7		9	59.9	86.4	93.3	79.9
	10	60.3	86.2	93.2	79.9		10	59.8	86.6	93.3	79.9		10	61.0	86.2	93.6	80.3
11	60.8	86.7	93.8	80.4	11	59.9	86.2	93.2	79.8	11	60.1	86.1	93.1	79.8			
9	0	59.5	86.2	93.0	79.6	10	0	60.2	86.7	93.4	80.1	11	0	61.4	87.4	93.4	80.7
	1	60.8	86.4	93.3	80.2		1	60.6	86.0	93.0	79.9		1	54.7	83.0	91.0	76.2
	2	60.4	86.8	93.4	80.2		2	60.7	85.6	93.3	79.9		2	59.3	84.9	91.9	78.7
	3	60.1	86.4	93.2	79.9		3	59.6	86.6	93.0	79.7		3	59.4	83.5	90.9	77.9
	4	59.8	86.2	92.7	79.6		4	61.0	86.9	93.4	80.4		4	60.2	86.2	93.2	79.9
	5	59.7	86.7	92.8	79.7		5	60.6	85.6	93.9	80.0		5	59.9	86.2	93.4	79.8
	6	60.8	87.2	93.4	80.5		6	60.6	86.8	93.2	80.2		6	61.5	87.1	94.6	81.1
	7	59.4	85.3	93.4	79.4		7	62.1	86.8	93.5	80.8		7	58.3	84.4	92.4	78.4
	8	61.2	86.5	93.5	80.4		8	60.9	86.7	93.4	80.3		8	58.1	84.6	92.3	78.3
	9	62.0	86.8	93.4	80.7		9	61.4	87.5	93.4	80.8		9	56.4	84.6	91.0	77.3
	10	60.4	86.7	93.4	80.2		10	61.1	86.2	93.4	80.2		10	60.6	86.7	93.6	80.3
11	60.0	86.8	93.3	80.0	11	61.6	86.8	93.1	80.5	11	59.2	85.0	91.9	78.7			
vanilla		60.4	86.2	93.2	79.9												

Table 19. Detailed text-to-image retrieval performance on the COCO-CN *val* set for each individually ablated head, evaluated using the ViT-B-based Chinese-CLIP model. Here, l denotes the l -th transformer layer of the image encoder, and h represents the h -th attention head in the multi-head attention (MHA) module. Evaluation metrics include recall rates at k (R@ k) and mean recall rate (mR). Results from the vanilla baseline are reported in the last row for reference.